2007 IEEE International Conference on
Robotics and Automation
Roma, Italy, 10-14 April 2007

Flagella-like Propulsion for Microrobots Using a Nanocoil and a Rotating Electromagnetic Field

D. J. Bell, *Student Member, IEEE,* S. Leutenegger, K. M. Hammar, L. X. Dong, *Member, IEEE,* and B. J. Nelson, *Senior Member, IEEE*

***Abstract*—A propulsion system similar in size and motion to the helical bacterial flagella motor is presented. The system consists of a magnetic nanocoil as a propeller (27 nm thick ribbon, 3 μm in diameter, 30-40 μm long) driven by an arrangement of macro coils. The macro coils generate a rotating field that induces rotational motion in the nanocoil. Viscous forces during rotation result in a net axial propulsion force on the nanocoil. Modeling of fluid mechanics and magnetics was used to estimate the requirements for such a system. The fabrication of the magnetic nanocoils and the system setup are explained. Experimental results from electromagnetic actuation of nanocoils as well as from their propulsion in both paraffin oil and water are presented. This is the first time a propulsion system of this size and motion-type has been fabricated and experimentally verified.**

I. Introduction

UNTETHERED microrobots have been proposed for a range of biological and biomedical applications. Due to the lack of suitable actuators and energy storage capabilities in microsystems, external energy transfer has usually been adopted, often by means of magnetic fields that are generated ex vivo. This has been used for the manipulation of magnetic devices in the body [1]. In addition, both DC fields with gradients [2-4] as well as rotating and oscillating fields [5-7] have been used to generate motion.

Another approach to propelling microrobots in liquid environments is to mimic the flagella motor, which has been an object of investigation for several decades. In 1952 Taylor [8] explored the swimming behavior of cells and bacteria. Since then there have been several other contributions in the exploration of flagella propulsion mainly through analysis and simulation. Most efforts aimed at estimating the power consumption and velocity of such organisms. Recently, real bacterial flagella were used to propel polystyrene beads [9]. Moreover, the beating flagella motion of eukaryotic cells was imitated with similar size [10]. However, imitation of the helical flagella motion of bacteria [11] with similar size has not been achieved yet, as the technology to fabricate suitable propellers was missing. With recent progress in the fabrication of nanocoils [12, 13], mimicking the natural propulsion strategy of bacterial flagella becomes feasible.

Manuscript received September 15, 2006. This work was supported by ETH Zurich.

The authors are with the Institute of Robotics and Intelligent Systems, ETH Zurich, CH-8092 Zurich, Switzerland (phone: +41-44-632-5529; fax: +41-44-632 1078; e-mail: bnelson@ethz.ch).

In this paper a novel propulsion system for microrobots with similar size and motion as bacterial flagella is demonstrated. It consists of a magnetic nanocoil and a setup of macro coils for the generation of the electromagnetic fields. The magnetic nanocoils can be fabricated with good control over their geometry. They consist of a 27 nm thick ribbon that, upon wet etch release, self-forms into a coil 3 μm in diameter with a length between 30 and 40 μm. A 2×2 μm^2, 200 nm thick magnetic plate is formed on one end that serves as a "head". First, a method is presented to estimate the forces from fluid mechanics acting on the nanocoils. From the results the torque requirements and the force output of the propulsion system can be estimated. Previous models for flagella hydrodynamics work with the assumption of a circular filament cross-section. Since the cross-sectional shape of the nanocoil ribbon used in this work is a high aspect-ratio rectangle, new models are needed. After some discussion of the relevant magnetics, the fabrication of the nanocoils is explained followed by a description of the remaining system setup. Next, experimental results are presented to demonstrate the propulsion concept.

II. Theory

A. Fluid Mechanics

The proposed propulsion system operates in the low Reynolds number regime where viscous forces dominate inertial forces [14]. Therefore, inertial and time-dependent terms in the Navier-Stokes equation can be neglected which results in the Stokes equation

$$\mu\Delta\vec{u} = \nabla p \tag{1}$$

where μ is the viscosity of the liquid, $\vec{u}$ is the velocity vector, and ∇p is the pressure gradient.

Expressions for the forces acting on a rotating helical micro- or nanostructure in low Reynold's number flow have been derived previously for structures with different cross-sectional geometries [15], such as circular cross-sections. However, for the high-aspect ratio, rectangular cross-section of the belt-like nanocoils used here, the models are not valid. In order to estimate the forces on these structures we propose to use the following numerical method as an efficient approximation. They can be computed by solving (1) and integrating the pressure as well as the

friction forces from Newton's equation for fluids (2) over its surface.

$$\tau_x = \mu \frac{\partial u_x}{\partial y} \tag{2}$$

where τ_x is the shear stress. The velocity field around the structure is required to compute the forces. In order to simplify the problem of the fluid flow around the rotating coil (Fig. 1a) the coil is treated as unwound and a length element is considered as illustrated in Fig. 1b. The fluid velocity on this moving element is decomposed into a tangential and a normal component. As a result two separate two-dimensional problems can be solved by introducing the scalar flow function Ψ and discretizing the equations. With the boundary conditions of zero flow at the surface of the cross-section and constant velocity at the boundaries of the simulation region a solution for the flow function and velocity components is found. A typical result for the streamlines around the cross-section of the ribbon is illustrated in Fig. 1. Next, the forces on the structures are computed by integrating pressure and shear stress over the entire body.

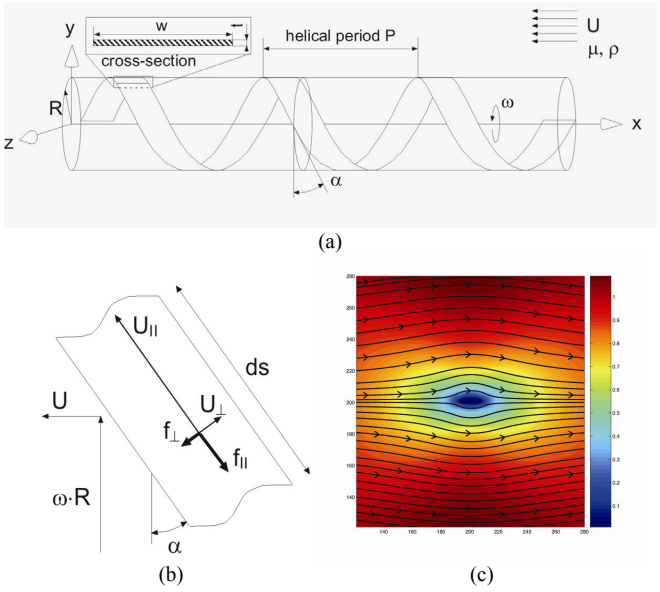

Fig. 1. (a) Schematic of nanocoil rotating in liquid with velocity and force components. (b) Schematic of unwound length element. (c) Result from numerical analysis. Streamlines and total fluid speed.

B. Magnetics

A magnetized volume V aligns with the direction of the magnetic field in which it is located. The torque T exerted to achieve this alignment is given by

$$T = V \cdot \vec{M} \times \vec{B} \tag{3}$$

where $\vec{M}$ is the magnetization and $\vec{B}$ is the magnetic flux density.

The magnetic flux density for a solenoid can be estimated with a dipole field model:

$$B_x(x) = \frac{\mu_0 \cdot m}{2\pi \cdot x^3} \tag{4}$$

where μ_0 is the permeability of free space, m is the dipole momentum, and x is the distance from the centre of the solenoid.

A Helmholtz coil generates a homogeneous field in its axial direction which is desirable in order to avoid translational magnetic forces from field gradients. The field strength can be estimated by

$$B_0 = \frac{\mu_0 I}{2R\left(5/4\right)^{3/2}} \tag{5}$$

where I is the current and R is the radius of the coil pair.

By superimposing sinusoidal fields of separate coils it is possible to generate a rotating DC field. The nanocoils have a thin soft magnetic plate attached to one end. Thus, a nanocoil rotates with the electromagnetic field if the axis of the nanocoil is aligned with the rotation direction of the electromagnetic field. The rotation of the electromagnetic field around any direction in space is illustrated schematically in Fig. 2. *B1* and *B2* represent the magnetic flux vectors at time 1 and 2. The angles α and β are used in the equations to determine the values of current in the three coil pairs of a 3-axes Helmholtz coil setup.

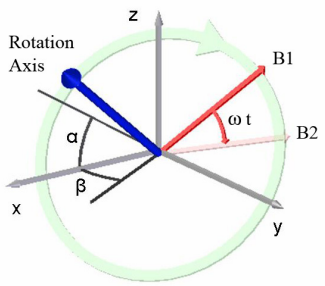

Fig. 2. Schematic illustration of the rotation of the electromagnetic field around any direction in space.

Electromagnetic simulation (Ansoft, Maxwell 3D) was used for the characterization of the macro coils. In the case of the three-axes Helmholtz coil it was used to estimate the inhomogeneity in the centre due to distortion of the field from the inner coils. In Fig. 3 the flux density of the field created by the large coil is plotted around the surface of the cubic sample volume in the centre. The changes over this surface are less than 0.5 % and the field gradient due to this inhomogeneity is less than 3 mT/m. The translational forces on the magnetic plates of the nanocoils from this field gradient are negligible.

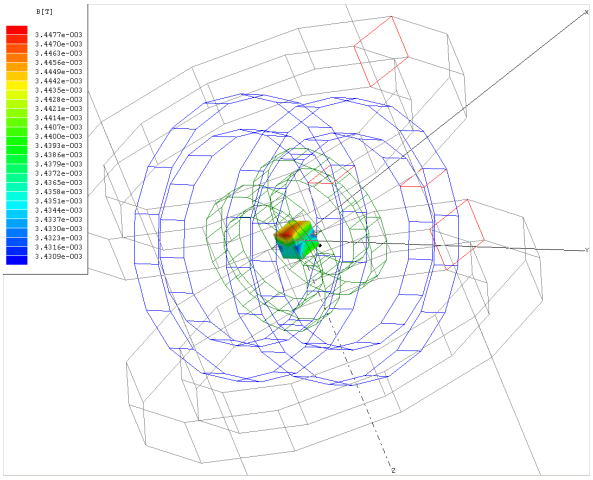

Fig. 3. Field strength around surface of sample volume.

III. Experimental

A. Magnetic Nanocoils

Figure 4 illustrates the fabrication process of the magnetic nanocoils. The initial layers were grown on semi-insulating GaAs (Freiberger Compound Materials) using a molecular beam epitaxy system (VEECO, Gen III MBE) equipped with a valved cracker for As and solid sources for Ga and In. Substrate temperature was determined by diffuse reflectance spectroscopy. Standard growth conditions were applied with a V/III ratio around 40 and growth rates of approximately 0.1 nm/s. A sacrificial layer of AlAs was grown onto a GaAs buffer layer at 580 °C. The subsequent 11nm thick InGaAs layer was deposited at 510 °C. An In content of 14 % was determined by X-ray diffraction measurements. The thickness of this layer must be smaller than the critical thickness to maintain elastic strain [16]. Finally, a 16 nm thick GaAs layer, n-type doped to $5 \cdot 10^{17}$ cm^{-3}, was deposited (Fig. 4a). The initial pattern in the bilayer can be created through positive photolithography (Fig. 4b). S1805 was used as a resist. After the development of the resist with MF319, RIE with a mixture of 95 sccm H_2 and 5 sccm CH_4 gases at a pressure of 130 µbar, a substrate temperature of 10 ˚C, and a power of 130 W was used to transfer the pattern to the InGaAs/GaAs bilayers at an etch rate of approximately 3.3 nm/s (Fig. 4c). Next, negative photolithography was used to create magnetic plates that are to be attached to the nanocoils. After exposure the ma-N1410 resist was developed in ma-D376XP (Fig. 4d). This developer is based on metasilicate and does not etch the underlying InGaAs/GaAs bilayer. Then, a 10 nm thick Cr adhesion layer and a 200 nm thick Ni layer are deposited through E-Beam evaporation (Fig. 4e). After lift-off in acetone, small plates of Ni remain on the tips of the bilayer strips (Fig. 4f). Next, 1 % HF aqueous solution was used to selectively etch the AlAs sacrificial layer under the InGaAs/GaAs heterostructures (Fig. 4g). During this wet etch, the patterned bilayer curled up along the nearest <100> direction releasing the internal strain and forming 3-D helical structures with Ni plates attached to the loose ends. The direction of the scrolling is determined by the anisotropy in stiffness of the InGaAs/GaAs bilayer. After the wet etch release the samples were rinsed in deionized water and subsequently in isopropyl alcohol. Finally, they were dried with a supercritical CO_2 dryer so that the structures would not be damaged from surface tension. A helical geometry can be achieved through this process if a rectangular shape is used as the initial planar pattern with an orientation at some angle relative to the nearest <100> direction.

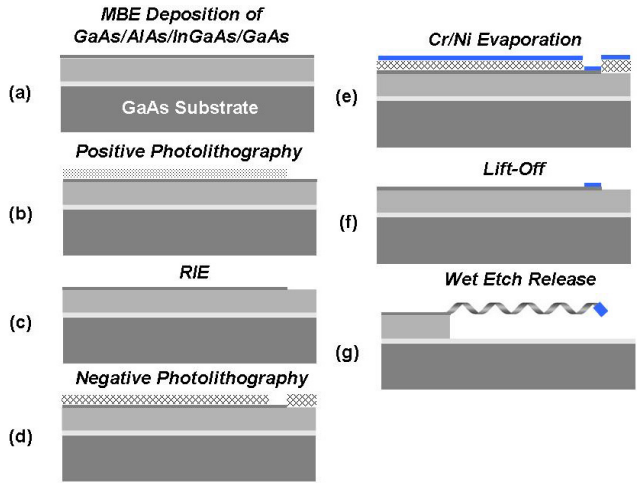

Fig. 4. Process sequence: initial planar, epitaxial bilayer with Ni parts, all patterned through conventional microfabrication techniques assembles itself into 3-D nanostructures during wet etch release.

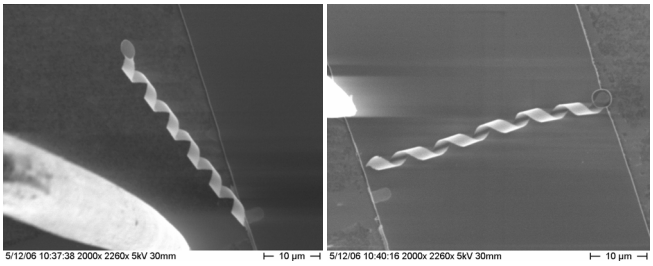

(a) (b)

Fig. 5. SEM images of nanocoil with Ni plate attached to one end before (a) and after (b) releasing. The probe tip on the manipulator that is used to break the attachment of individual coils to the chip is also visible.

After this fabrication process arrays of nanocoils are fixed to the chip on one side. An SEM image of one nanocoil fixed to the chip is shown in Fig. 5a. In order to have individual coils suspended in liquid their attachment to the chip has to be broken. For this purpose a nanomanipulator (Kleindiek, MM3A), was installed inside an SEM (Zeiss, DSM 962). A tungsten probe (Picoprobe, T-4-10-1mm) with a tip radius of 100 nm mounted on the nanomanipulator was then used to break the attachment of the coils (Fig. 5b). The tip is visible on both images in Fig. 5. Afterwards the chip with these coils lying on the surface was put into a holder that could be inserted into the centre of the setup of macro coils. The cavity in which the chip was placed was filled with paraffin oil or

water. The advantage of using paraffin oil rather than water is that it is less volatile, so that the experiments can be conducted without a cover. However, a higher torque than in water is required.

B. *Electromagnetic Field Generation*

For the generation of the electromagnetic field two different setups of macro coils were constructed. They are shown in Figs. 6 and 7. The first setup consists of four coils with ferrite cores (Fig. 6a). It can be used to create a field that rotates around one axis only. At any time the current was going in the same direction for coils opposite to each other. This resulted in a low field gradient in the center, as shown in Fig. 6b. The magnetic flux density is plotted for the measured value in the center, the dipole model, and for simulation results. The maximum current through each coil in the experiments was 1.5 A which resulted in a maximum field strength of 40 mT in the center. Real-time feed-forward controlled sinusoidal output current with four output channels was generated with the S626 Sensoray Board as well as three power amplifiers (Maxon Motor) set to current output mode. The DAC output voltage range of ± 10 V is translated into an output current between -1.5 and +1.5 A. A C program generates the current output.

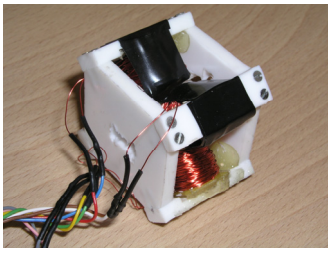

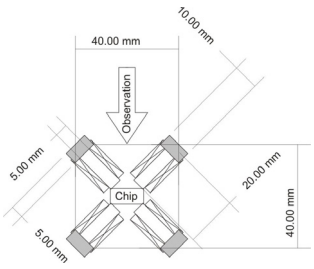

(a)

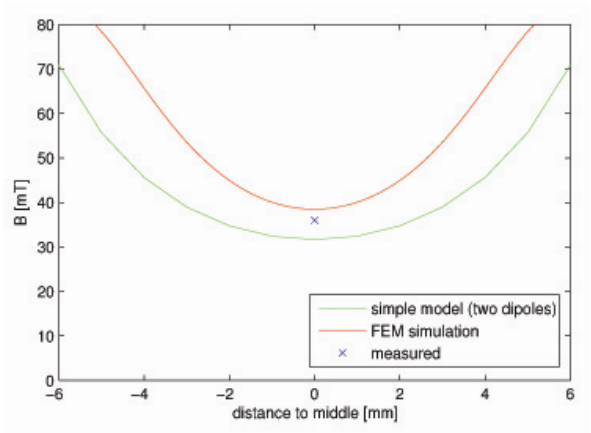

(b)

Fig. 6. (a) Image and (b) Schematic of setup of macro coils for rotation around one axis. (c) Magnetic flux density between two opposite solenoids for a current of 1.5 A.

The second design consists of three Helmholtz coils. With this setup a DC field that rotates around any direction in space can be generated. Moreover, with the use of Helmholtz coils the homogeneity of the field is improved so that any translational magnetic forces are minimized. An image and a schematic of the coil setup is shown in Fig. 7a and 7b, respectively. The coils are designed so that there is enough space for the focus of the 50x objective of the microscope to reach the whole sample volume in the centre of the coils. The small, medium, and large Helmholtz coils have 170, 320, and 500 turns of a 0.35 mm Cu wire, respectively. The maximum current is around 0.4 A. The same card and amplifiers are used with the three-axis Helmholtz coil setup. The DAC output voltage range of ± 10 V is translated into an output current between -0.4 and +0.4 A. Again a C program generates the current output. The input to the program is the initial direction of rotation, the maximum field strength up to 2 mH, and the rotational velocity of the field. During operation it is possible to adjust the direction of rotation. The three Helmholtz coils were calibrated with a gaussmeter to generate the same maximum field strength. Images and videos were taken with a camera mounted on top of the microscope. A block diagram of the whole propulsion system is illustrated in Fig. 7c.

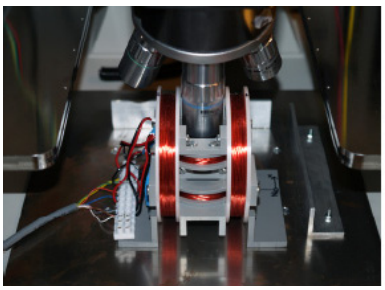

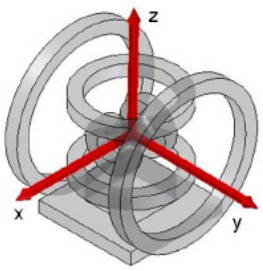

(a) (b)

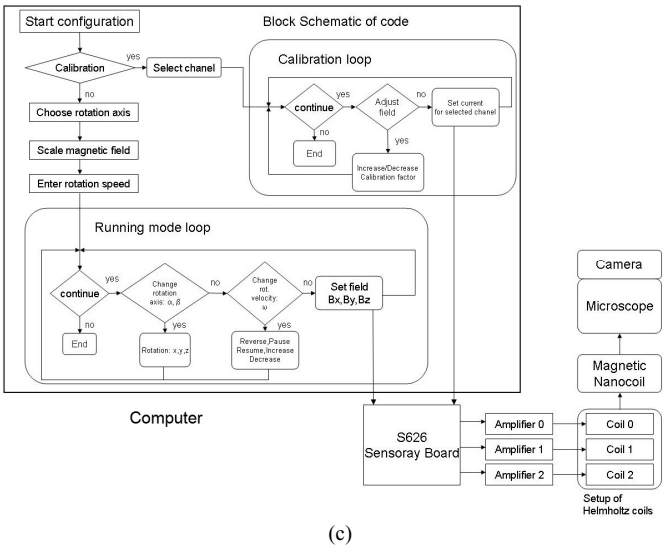

(c)

Fig. 7. Three-axes Helmholtz coil setup for rotation of field in arbitrary direction. (a) Image of setup under microscope (b) Schematic. (c) System block diagram.

IV. Results

The first experiments were done with the coil setup presented in Fig. 6. As a first experiment, nanocoils that were still attached to the chip on one side were actuated. The deflections were observed with an optical microscope at a magnification of 50x. In Fig. 8a images are shown with the nanocoils in torsion due to different magnetic flux densities. The green arrows indicate the flux direction. The blue arrows on the magnetic plates are an estimate of the magnetization direction. Due to its small thickness the magnetization direction is always in the plane of the magnetic plate. In Fig. 8b a plot of the tip orientation of the coil versus the magnetic flux density is shown. The values for the coil tip orientation were estimated from the images. A torsion spring model was fitted to the experimental data with a value for the torsional spring constant of $4.5 \cdot 10^{-14}$ Nm. From these results it could be demonstrated that the rotation of the nanocoils with magnetic fields can be achieved. The torque required to rotate the structure in liquid is much lower than the torque that was used to achieve these torsional displacements.

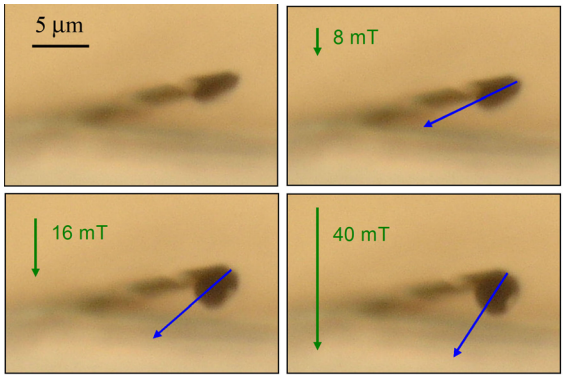

(a)

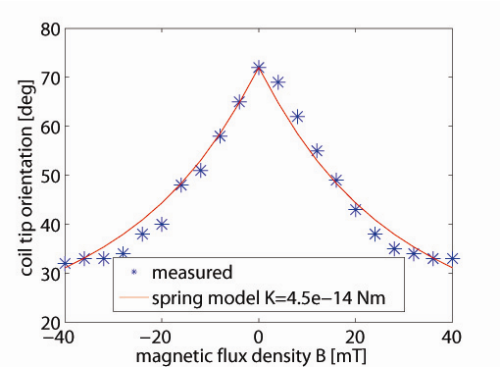

(b)

Fig. 8. Torsion of nanocoil attached to the chip on one side by applying different values of field strength. (a) Optical microscope images. The green arrows indicate the flux direction. The blue arrows on the magnetic plates are an estimate of the magnetization direction. (b) Angular orientation of Ni plate attached to nanocoil as a function of the applied *B* field. A torsion spring model is fitted to the experimental results.

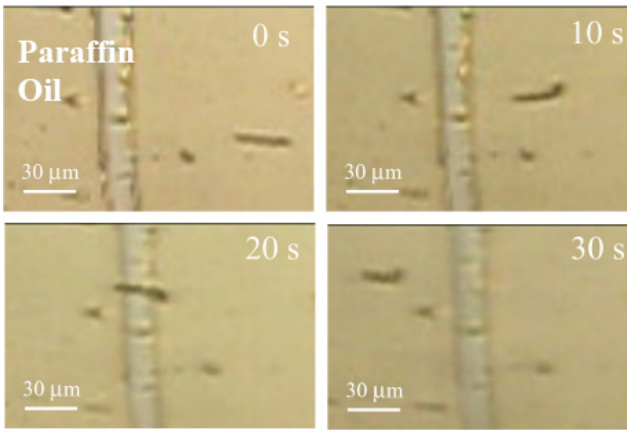

(a)

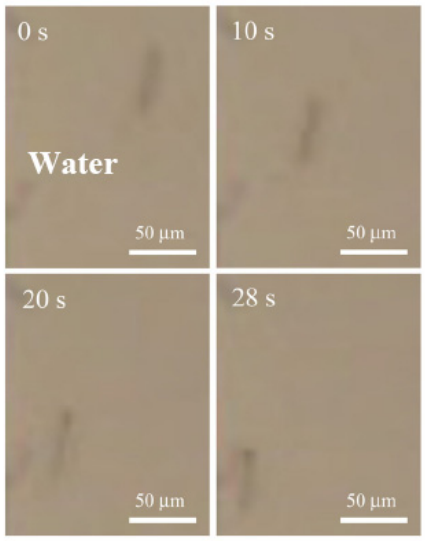

(b)

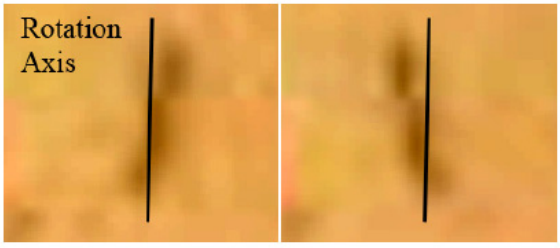

(c)

Fig. 9. Nanocoils are rotating in liquid with the electromagnetic field which results in an axial forward motion. (a) Sequence 1: 30 µm long coil in oil. Also visible is a part of the pattern on the surface of the chip. (b) Sequence 2: 40 µm long coil in water. (c) Images indicating motion during one rotation in sequence 2.

For the first propulsion experiment individual magnetic nanocoils were immersed in paraffin oil, as outlined in section III-A. They were then actuated with the rotating electromagnetic field and their motion was captured on video through the microscope. In Fig. 9a one sequence of nanocoil propulsion is illustrated. Images after different time intervals

are shown. The time for one rotation is 0.39 s. Therefore, the rotational velocity is 16.3 rad/s or 158 rpm. The length of the coil is around 30 μm. Therefore, it can be estimated from Fig. 9a that the axial velocity is approximately 3.9 μm/s. The filament rotation of bacterial flagella in water typically reaches between 200 and 1000 rpm.

It was also possible to conduct experiments with nanocoils immersed in water. In these experiments the three-axis Helmholtz coils was used for the actuation of the nanocoils. The experimental procedure was more difficult than with oil. The volume of water had to be small in order to locate individual nanocoils. Therefore, the water evaporated relatively quickly and had to be refilled regularly during the experiments. Moreover, in water it was more difficult to have individual nanocoils floating some distance over the surface. Magnets and micropositioners with probes attached were used to achieve this. In Fig. 9b images of a nanocoil swimming in water at different time intervals are shown. It can be seen from these images that the movement does not happen exactly in the axial direction. Instead there is a small component of motion in the transverse direction. The nanocoil in this case was moving too close to the surface of the chip. This probably induced some transverse force. The rotational velocity is 6.3 rad/s or 60 rpm. The length of the coil is 40 μm. Therefore, it can be estimated from Fig. 9 that the axial velocity is 4.6 μm/s. In Fig. 9c two images are shown to illustrate the motion during one rotation of the nanocoils in Fig. 9b. The rotational motion of the nanocoil can be considered as a superposition of rotation around its axis and rotation of the end with the Ni plate attached around the axis of rotation of the electromagnetic field.

V. Conclusion

The feasibility of propelling microrobots using magnetic nanocoils and rotating external electromagnetic fields has been demonstrated. Thus, the helical propulsion of bacterial flagella could be imitated for the first time with similar size. The nanocoils can be actuated remotely when they are functionalized with a magnetic plate on one end. The fabrication process has been described. With this system rotational velocities between 55 and 158 rpm resulted in axial velocities between 2.3 and 3.9 μm/s in paraffin oil. In water, a rotational velocity of 60 rpm resulted in an axial velocity of 4.6 μm/s. A method was presented to estimate the torque requirements and the force output for nanocoils with high aspect ratio, rectangular cross-sections.

Unlike previous concepts for micropropulsion, nanocoil propellers are also suitable for self-propulsion as would be required for fully autonomous microrobots in combination with an internal energy supply and nano- or microactuators such as biomolecular motors [17, 18].

References

[1] G. T. Gillies, R. C. Ritter, W. C. Broaddus, M. S. Grady, M. A. Howard, and R. G. Mcneil, "Magnetic Manipulation Instrumentation for Medical Physics Research," *Review of Scientific Instruments*, vol. 65, pp. 533-562, 1994.

[2] M. B. Khamesee, N. Kato, Y. Nomura, and T. Nakamura, "Design and control of a microrobotic system using magnetic levitation," *IEEE-ASME Transactions on Mechatronics*, vol. 7, pp. 1-14, 2002.

[3] J. B. Mathieu, S. Martel, L. Yahia, G. Soulez, and G. Beaudoin, "Preliminary investigation of the feasibility of magnetic propulsion for future microdevices in blood vessels," *Bio-Medical Materials and Engineering*, vol. 15, pp. 367-374, 2005.

[4] K. B. Yesin, K. Vollmers, and B. J. Nelson, "Modeling and control of untethered biomicrorobots in a fluidic environment using electromagnetic fields," *International Journal of Robotics Research*, vol. 25, pp. 527-536, 2006.

[5] K. Ishiyama, K. I. Arai, M. Sendoh, and A. Yamazaki, "Spiral-type micromachine for medical applications," presented at International Symposium on Micromechatronics and Human Science, 2000.

[6] T. Mei, Y. Chen, G. Fu, and D. Kong, "Wireless drive and control of a swimming microrobot," presented at IEEE International Conference on Robotics and Automation, 2002.

[7] M. Sendoh, N. Ajiro, K. Ishiyama, M. Inoue, K. I. Arai, T. Hayase, and J. Akedo, "Effect of machine shape on swimming properties of the spiral-type magnetic micro-machine," *IEEE Transactions on Magnetics*, vol. 35, pp. 3688-3690, 1999.

[8] G. Taylor, "The Action of Waving Cylindrical Tails in Propelling Microscopic Organisms," *Proceedings of the Royal Society of London Series A-Mathematical and Physical Sciences*, vol. 211, pp. 225-239, 1952.

[9] B. Behkam and M. Sitti, "Bacterial flagella-based propulsion and on/off motion control of microscale objects," *Applied Physics Letters*, vol. 90, art. no.. 023902, 2007.

[10] R. Dreyfus, J. Baudry, M. L. Roper, M. Fermigier, H. A. Stone, and J. Bibette, "Microscopic artificial swimmers," *Nature*, vol. 437, pp. 862-865, 2005.

[11] H. C. Berg and R. A. Anderson, "Bacteria Swim by Rotating Their Flagellar Filaments," *Nature*, vol. 245, pp. 380-382, 1973.

[12] V. Y. Prinz, V. A. Seleznev, A. K. Gutakovsky, A. V. Chekhovsky, V. V. Preobrazhenskii, M. A. Putyato, and T. A. Gavrilova, "Free-standing and overgrown InGaAs/GaAs nanotubes, nanohelices and their arrays," *Physica E*, vol. 6, pp. 828-831, 2000.

[13] D. J. Bell, L. X. Dong, L. Zhang, M. Golling, B. J. Nelson, and D. Gruetzmacher, "Fabrication and characterization of three-dimensional InGaAs/GaAs nanosprings," *Nano Lett.*, vol. 6, pp. 725-729, 2006.

[14] E. M. Purcell, "Life at low Reynolds numbers," *American Journal of Physics*, vol. 45, pp. 3-11, 1977.

[15] J. Gray and G. J. Hancock, "The Propulsion of Sea-Urchin Spermatozoa," *Journal of Experimental Biology*, vol. 32, pp. 802-814, 1955.

[16] A. Sasaki, "Initial growth layers and critical thickness of InAs heteroepitaxy on GaAs substrates," *Journal of Crystal Growth*, vol. 160, pp. 27-35, 1996.

[17] R. K. Soong, G. D. Bachand, H. P. Neves, A. G. Olkhovets, H. G. Craighead, and C. D. Montemagno, "Powering an inorganic nanodevice with a biomolecular motor," *Science*, vol. 290, pp. 1555-1558, 2000.

[18] B. S. Lee, S. C. Lee, and L. S. Holliday, "Biochemistry of mechanoenzymes: Biological motors for nanotechnology," *Biomedical Microdevices*, vol. 5, pp. 269-280, 2003.